HHS Public Access

Author manuscript

Adv Nanobiomed Res. Author manuscript; available in PMC 2023 July 01.

Published in final edited form as:

Adv Nanobiomed Res. 2022 July ; 2(7): . doi:10.1002/anbr.202200022.

Methacrylate-Modified Gold Nanoparticles Enable Non-Invasive Monitoring of Photocrosslinked Hydrogel Scaffolds

Lan Li[1,2], **Carmen J. Gil**[3], **Tyler A. Finamore**[1], **Connor J. Evans**[1], **Martin L. Tomov**[3], **Liqun Ning**[3], **Andrea Theus**[3], **Gabriella Kabboul**[3], **Vahid Serpooshan**[3,4], **Ryan K. Roeder**[1,2]

[1]Department of Aerospace and Mechanical Engineering, Bioengineering Graduate Program, Materials Science and Engineering Graduate Program, University of Notre Dame, Notre Dame, IN 46556, USA

[2]Notre Dame Center for Nanoscience and Technology (ND*nano*), University of Notre Dame, Notre Dame, IN 46556, USA

[3]Wallace H. Coulter Department of Biomedical Engineering, Georgia Institute of Technology, Atlanta, GA 30332, USA

[4]Department of Pediatrics, Emory University School of Medicine, Emory University, Atlanta, GA 30322, USA

Abstract

Photocrosslinked hydrogels, such as methacrylate-modified gelatin (gelMA) and hyaluronic acid (HAMA), are widely utilized as tissue engineering scaffolds and/or drug delivery vehicles, but lack a suitable means for non-invasive, longitudinal monitoring of surgical placement, biodegradation, and drug release. Therefore, we developed a novel photopolymerizable X-ray contrast agent, methacrylate-modified gold nanoparticles (AuMA NPs), to enable covalent-linking to methacrylate-modified hydrogels (gelMA and HAMA) in one-step during photocrosslinking and non-invasive monitoring by X-ray micro-computed tomography (micro-CT). Hydrogels exhibited a linear increase in X-ray attenuation with increased Au NP concentration to enable quantitative imaging by contrast-enhanced micro-CT. The enzymatic and hydrolytic degradation kinetics of gelMA-Au NP hydrogels were longitudinally monitored by micro-CT for up to one month *in vitro*, yielding results that were consistent with concurrent measurements by optical spectroscopy and gravimetric analysis. Importantly, AuMA NPs did not disrupt the hydrogel network, rheology, mechanical properties, and hydrolytic stability compared with gelMA alone. GelMA-Au NP hydrogels were thus able to be bioprinted into well-defined three-dimensional

Correspondence: Ryan K. Roeder, Ph.D., Professor, Department of Aerospace and Mechanical Engineering, Bioengineering Graduate Program, 148 Multidisciplinary Research Building, University of Notre Dame, Notre Dame, IN 46556, Phone: (574) 631-7003, rroeder@nd.edu.

Author Contributions

L.L., C.J.G., V.S and R.K.R. designed experiments, analyzed data, and wrote the manuscript. L.L. and C.J.G. were primarily responsible for performing all experiments. T.A.F., C.J.E., L.N., M.L.T., A.T., and G.K. provided assistance in performing experiments and editing the manuscript.

Supporting Information

Supporting Information to this article is available from the Wiley Online Library or from the author.

Conflict of Interest

The authors declare no conflict of interest.

architectures supporting endothelial cell viability and growth. Overall, AuMA NPs enabled the preparation of both conventional photopolymerized hydrogels and bioprinted scaffolds with tunable X-ray contrast for noninvasive, longitudinal monitoring of placement, degradation, and NP release by micro-CT.

Keywords

Computed Tomography; Gelatin Methacryloyl (GelMA) Hydrogel; Gold Nanoparticles; Photopolymerization; Tissue Engineering Scaffold

1. Introduction

Photocrosslinked hydrogels, such as methacrylate-modified gelatin (gelMA),[1–3] hyaluronic acid (HAMA),[4–6] and collagen (colMA),[7–9] are widely utilized as tissue engineering scaffolds and drug delivery vehicles due to enabling precision manufacturing (e.g., 3D printing) of biodegradable materials with tunable properties, and the incorporation of sensitive cells and/or biomolecules.[10,12] However, there is currently no established means for noninvasive, longitudinal, and volumetric monitoring of hydrogel scaffolds once implanted *in vivo*. Conventional methods to longitudinally monitor scaffold degradation and integration, such as histology and mechanical testing, require invasive excision of multiple tissue samples.[13] Therefore, various imaging modalities have been investigated for noninvasive assessment of hydrogel degradation and drug delivery,[13,14] including ultrasound elasticity imaging,[15,16] photoacoustic imaging,[17,18] near-infrared fluorescence imaging,[19–24] magnetic resonance imaging (MRI),[24–27] and X-ray computed tomography (CT).[28–30] Among these, CT imaging is advantageous in providing low cost, three-dimensional (3D), deep tissue imaging at high spatial and temporal resolution, but is limited by low soft tissue contrast.

CT imaging contrast is derived from the X-ray attenuation of the scaffold material relative to adjacent tissue.[31] Hydrogels and other soft biomaterials exhibit similar X-ray attenuation to soft tissues and thus low X-ray contrast.[13] Therefore, contrast agents are required to overcome this limitation. Gold nanoparticles (Au NPs) have become the most widely utilized X-ray contrast agent in preclinical research due to exhibiting strong X-ray attenuation while facilitating facile synthesis and surface modification.[31,32] Therefore, the incorporation of Au NPs within photocrosslinked hydrogels could enable non-invasive, post-operative imaging of surgical placement and longitudinal, quantitative imaging of degradation and/or drug delivery. However, the method by which Au NPs are integrated into a hydrogel is crucial for achieving the desired functionality.[33–35]

Au NPs have been incorporated within hydrogels by physical and chemical means.[33–35] In physical incorporation, Au NPs are mixed into the prepolymer solution and entrapped within the hydrogel during crosslinking.[36–38] Physical incorporation is simple and flexible but may suffer from disrupting the hydrogel network and properties, including premature or uncontrolled (burst) release of NPs which limits the effective time for longitudinally monitoring hydrogel function.[36–39] In chemical incorporation, Au NPs are surface functionalized with ligands that are able to be chemically-coupled to hydrogel

macromolecules.[29,35,40,41] Chemically-incorporated NPs are immobilized such that their release coincides with hydrolytic or enzymatic degradation of the hydrogel for accurate and reliable monitoring.[29] However, the chemical incorporation of NPs in hydrogels typically requires modification of both NP surfaces and hydrogel macromolecules, involving multi-step reactions with potentially undesirable side reactions, prior to photocrosslinking the hydrogel.[40–43] Thus, simple and flexible methods are needed for the chemical incorporation of Au NPs in photocrosslinked hydrogels with minimal disruption of the hydrogel structure and properties.

Therefore, the objective of this study was to investigate a photopolymerizable X-ray contrast agent, methacrylate-modified Au NPs (AuMA NPs), which can be directly conjugated to methacrylate-modified hydrogels (gelMA and HAMA) in one-step during photocrosslinking to subsequently enable non-invasive, longitudinal monitoring of scaffold degradation and/or drug delivery. GelMA-Au NP hydrogels prepared by one-step photopolymerization (1-step gelMA-Au) were compared with gelMA alone, gelMA with physically-entrapped Au NPs (gelMA+Au), and gelMA chemically-coupled with Au NPs using carbodiimide/succinimide (EDC/NHS) chemistry prior to photocrosslinking (2-step gelMA-Au) (Figure 1). The effective swelling ratio, mechanical properties and degradability of photocrosslinked gelMA-Au NP hydrogels and the rheological properties of bioinks were characterized and compared with normal gelMA. The hydrolytic and enzymatic degradation kinetics of gelMA-Au NP hydrogels were measured longitudinally by contrast-enhanced micro-CT, and compared with concurrent measurements by optical spectroscopy and gravimetric analysis. In addition, gelMA-Au NP bioinks were printed into 3D architectures and loaded with endothelial cells to evaluate cell viability.

2. Results and Discussion

2.1. Synthesis and Characterization of AuMA NPs

AuCOOH NPs were first prepared by the citrate reduction method followed by surface functionalization with mercaptosuccinic acid.[29,44] AuMA NPs were then prepared by covalently-linking AuCOOH NPs with 2-aminoethyl methacrylate (AEMA) using carbodiimide/succinimide (EDC/NHS) chemistry (Figure 2a). The molar ratio of Au:EDC:NHS:AEMA was set at 1:15:6:6 to maximize the conjugation efficacy of AuCOOH NPs and AEMA, while maintaining solubility and colloidal stability of AuMA NPs in aqueous solution for at least two weeks after synthesis. A higher degree of methacrylation (e.g., Au:EDC:NHS:AEMA = 1:75:30:30) was also investigated, but resulted in more hydrophobic NPs which settled out of solution within 2 days after synthesis.

As-prepared AuMA NPs remained spherical and monodispersed with a mean (± standard deviation) diameter of 12.2 (1.2) nm, similar to the initial citrate-stabilized Au NPs and AuCOOH NPs,[29,44] as measured by transmission electron microscopy (TEM) (Figure 2b). Aqueous colloidal stability of AuMA NPs was verified by dynamic light scattering (DLS) and zeta potential compared with AuCOOH NPs. The mean (± standard deviation) hydrodynamic diameter of AuMA and AuCOOH NPs was 91.4 (8.0) and 20.3 (1.4) nm (Figure 2c), and the mean (± standard deviation) zeta potential was −30.9 (1.1) and −13.0 (2.1) mV (Figure 2d), respectively. The greater hydrodynamic diameter after methacrylation

is explained by the association of hydrophobic ligands in aqueous solution, resulting in the formation of dispersible nanoclusters observed in TEM (Figure 2b). The increased magnitude of negative zeta potential with increased hydrodynamic diameter was previously observed for other functionalized Au NPs.[45]

The long-term colloidal stability of AuMA NPs in aqueous solution was monitored by DLS. The hydrodynamic diameter and polydispersity index of AuMA NPs remained unchanged at ~100 nm and ~0.2, respectively, after at least 40 days of storage when redispersed by ultrasonication. When redispersed by vortexing, the hydrodynamic diameter increased to ~100 nm after 7 days, but the polydispersity index remained unchanged at ~0.2. These results confirmed that AuMA nanoclusters observed in TEM were redispersible and stable during long-term storage.

Methacrylate surface modification was verified by Fourier-transform infrared spectroscopy (FTIR) and nuclear magnetic resonance (NMR) spectroscopy of as-prepared AuMA NPs compared with AEMA molecules. The FTIR spectra of AuMA NPs exhibited characteristic peaks for methacrylate ligands at 1635 cm^{-1} (C=C) and 854 cm^{-1} (=CH), as well as the amide linkage formed by conjugation of AEMA to AuCOOH NPs at ~1650 cm^{-1} (Amide I, C=O stretch), ~1540 cm^{-1} (Amide II, N-H bend and C-N stretch), and ~1230 cm^{-1} (Amide III, N-H in-plane bend and C-N stretch) (Figure 2e), which suggested successful conjugation of AEMA to AuCOOH NPs. ^{1}H NMR spectra also confirmed methacrylate surface modification via characteristic peaks at approximately 4.2, 3.7, and 1.9 ppm (Figure 2f). Characteristic peaks for vinylic protons at approximately 5.7 and 6.1 ppm were not observed for AuMA NPs, but the disappearance and broadening of peaks is commonly observed for small molecules attached to NP surfaces.[46]

2.2. Preparation of GelMA-Au NP Photopolymerized Hydrogels

GelMA-Au NP hydrogels were prepared by one-step photopolymerization (1-step gelMA-Au) with AuMA NPs and compared with gelMA alone, gelMA with physically-entrapped Au NPs (gelMA+Au), and gelMA chemically-coupled with Au NPs using EDC/NHS chemistry prior to photocrosslinking (2-step gelMA-Au) (Figure 1). AuMA NPs enabled the preparation of chemically-coupled gelMA-Au NP hydrogels in one-step by photopolymerization after simply mixing AuMA NPs with gelMA prepolymer solutions, similar to physical mixing (gelMA+Au). In contrast, chemical-coupling of AuCOOH NPs to gelMA using EDC/NHS chemistry required two separate steps for chemical-coupling and photocrosslinking (2-step gelMA-Au).

2.2.1. Rheology of Prepolymer Solutions—Prepolymer solutions for 1-step gelMA-Au hydrogels exhibited the most similar rheological properties compared with gelMA alone (Figure S2). Both 1-step gelMA-Au and gelMA+Au prepolymer solutions did not alter the sol-gel transition temperature of gelMA (Figure S2a,b). In contrast, 2-step gelMA-Au prepolymer solutions lost a thermal sol-gel transition when efficient chemical-coupling of Au-COOH NPs to gelMA macromolecules was assured by using an excess of EDC/NHS. Two-step gelMA-Au prepolymer solutions prepared with a Au:EDC:NHS molar ratio of 1:160:64 did not exhibit a thermal sol-gel transition when heated as high as 80°C, most

likely due to EDC/NHS-mediated crosslinking of amine and carboxylate ligands on gelMA macromolecules. Two-step gelMA-Au prepolymer solutions prepared with a Au:EDC:NHS molar ratio of 1:1:1 were able to achieve a sol-gel transition temperature comparable to gelMA alone (Figure S2a,b), but only with compromised efficiency for chemical-coupling AuCOOH NPs to gelMA and disruption of the photocrosslinked hydrogel network, as shown below.

GelMA and gelMA-Au NP prepolymer solutions all exhibited shear thinning with increased shear rate ($p < 0.0.001$, ANCOVA), as expected (Figure S2c). One-step gelMA-Au prepolymer solutions exhibited a lower apparent viscosity compared with gelMA overall ($p < 0.05$, Tukey), but meaningful differences were primarily at low shear rates ($< 10\ s^{-1}$). At higher shear rates ($> 10\ s^{-1}$) relevant to 3D printing processes, gelMA and 1-step gelMA-Au prepolymer solutions exhibited similar apparent viscosity (Figure S2c). In contrast, gelMA+Au and 2-step gelMA-Au prepolymer solutions exhibited lower apparent viscosity compared with both gelMA and 1-step gelMA-Au prepolymer solutions overall ($p < 0.05$, Tukey), and especially at higher shear rates.

2.2.2. Optimization of Photocrosslinking—The concentration of Au NPs in gelMA-Au NP hydrogels was recognized to exhibit competing effects on X-ray contrast and photocrosslinking. Greater concentrations of Au NPs enable greater absorption of X-rays, [31] which is beneficial for radiographic contrast, but also increase the absorption and scattering of ultra-violet (UV) and visible light,[47] which inhibits photocrosslinking (Table S1). Therefore, photocrosslinking studies were performed to optimize key parameters – including the Au NP concentration; photoinitiator type, concentration, and incubation time; gelMA concentration; and UV light intensity and irradiation time – for achieving fully crosslinked hydrogels with sufficient radiographic contrast, while minimizing the UV irradiation intensity and time to avoid damage to encapsulated cells and/or biomolecules.

GelMA+Au NP hydrogels prepared with 10% w/v gelMA, 0.5% w/v Irgacure photoinitiator, and 0–22 mM Au NPs initially revealed that hydrogels containing up to 7 mM Au NPs were fully crosslinked and hydrogels containing at least 15 mM Au NPs exhibited little or no crosslinking under UV irradiation at 7 and 15 mW/cm^2 for 6 min (Table S1). Therefore, a subsequent study systematically investigated increased photoinitiator concentration (1.0% w/v Irgacure 2959) and UV light intensity (30 mW/cm^2, 4 min), but gelMA+Au NP hydrogels containing more than 7 mM Au NPs were still not fully crosslinked (Table S2). These results, and the inability to improve photocrosslinking with increased photoinitiator concentration and UV light intensity, suggested that the effective UV intensity for activating the photoinitator was reduced by absorption and scattering from Au NPs.

One-step gelMA-Au NP hydrogels prepared under conditions previously shown to result in little or no crosslinking in gelMA+Au NP hydrogels (Table S2) also exhibited little or no photocrosslinking using 10% w/v gelMA, but exhibited improved crosslinking using 20% w/v gelMA, with either 15 or 37 mM Au NPs (Table S3). The increased gelMA concentration increased the number of potential crosslinking sites and their proximity with the photoinitiator without a loss in transparency for UV light penetration. Finally, lithium phenyl-2,4,6-trimethylbenzoylphosphinate (LAP) was investigated as an alternative

photoinitiator known to exhibit more rapid photopolymerization kinetics and higher water solubility compared to Irgacure 2959.[48,49] LAP improved photocrosslinking of 1-step gelMA-Au hydrogels prepared with 20% w/v gelMA and up to 37 mM Au NPs compared to Irgacure, especially after incubating prepolymer solutions with the photoinitiator for at least 24 h prior to photocrosslinking (Table S4). This result suggests that in addition to absorbing and scattering of UV light AuMA NPs may have inhibited photocrosslinking due to increasing the hydrophobicity prepolymer solutions. Importantly, 1-step gelMA-Au hydrogels comprising up to 10 and 37 mM AuMA NPs were fully crosslinked after incubating prepolymer solutions with 0.5% w/v LAP for 24 h and 7 d, respectively, and photocrosslinking under UV irradiation at 30 mW/cm^2 for 4 min (Table S4).

In summary, challenges to achieving fully crosslinked gelMA-Au NP hydrogels were circumvented by increasing the gelMA concentration, adopting LAP as the photoinitiator, and incubating prepolymer solutions with LAP for at least 24 h prior to photocrosslinking. GelMA and gelMA-Au NP hydrogels described hereafter were prepared with 20% w/v gelMA and up to 37 mM Au NPs by incubating prepolymer solutions with 0.5% w/v LAP photoinitiator 24 h at 4°C and photocrosslinking under UV irradiation at 30 mW/cm^2 for 4 min. Photocrosslinking under these conditions was verified by a surface photocrosslinking experiment between gelMA and AuMA NPs, as well as gelMA and AuCOOH NPs as a negative control. AuMA NPs were photocrosslinked to the surface of gelMA hydrogels and remained attached after thorough washing, while AuCOOH NPs were removed by washing after photocrosslinking (Figure S3). This result suggests that gelMA and AuMA NPs were able to be covalently-linked during photocrosslinking.

2.3. Characterization of GelMA-Au NP Hydrogels

2.3.1. X-Ray Contrast—GelMA-Au NP hydrogels were prepared by the one-step photocrosslinking strategy with varying concentrations of AuMA NPs to determine a suitable Au NP concentration for longitudinal monitoring of hydrogels by micro-CT. The X-ray attenuation of as-prepared 1-step gelMA-Au hydrogels increased linearly with increasing Au NP concentration ($p < 0.001$) and was strongly correlated ($R^2 = 0.99$), as expected (Figure 3a). This result confirmed that AuMA NPs can provide tunable X-ray contrast in gelMA hydrogels to enable quantitative imaging by micro-CT. GelMA-Au NP hydrogels containing at least 5 mM Au NPs exhibited sufficient X-ray attenuation for contrast enhancement ($\Delta HU \geq 30$[50]) versus soft tissue (Figure 3a), as represented by PBS (38.3 HU) and myocardium tissue (−9.3 HU). Grayscale micro-CT images of hydrogels containing at least 5 mM Au NPs exhibited visibly greater X-ray attenuation compared with PBS (Figure 3a). However, the concentration of Au NPs within a fixed volume was anticipated to decrease over time with hydrogel degradation and Au NP release. Therefore, a concentration of 10 mM Au NPs was chosen to provide ample X-ray contrast versus soft tissue for monitoring degradation through the entire hydrogel lifetime.

2.3.2. Swelling Ratio—The effective swelling ratio of gelMA-Au NP hydrogels was measured and compared to gelMA alone to evaluate the hydrogel crosslinking density. The effective swelling ratio of 1-step gelMA-Au hydrogels was not statistically different ($p > 0.48$, Tukey) from gelMA alone (Figure 3b). In contrast, physically-mixed gelMA+Au

hydrogels and 2-step gelMA-Au hydrogels exhibited a greater swelling ratio compared to gelMA alone ($p < 0.05$, Tukey). These results suggest that 1-step gelMA-Au hydrogels prepared with AuMA NPs did not disrupt the hydrogel network or crosslinking density compared with gelMA alone. AuMA NPs provided numerous ligands for photocrosslinking into the gelMA hydrogel network (Figure 1a). In contrast, physically-mixed gelMA+Au hydrogels and 2-step gelMA-Au hydrogels disrupted the hydrogel network and/or reduced the crosslinking density compared with gelMA alone. In physically-mixed gelMA+Au hydrogels, AuCOOH NPs were unable to participate in photocrosslinking and thus disrupted the gelMA hydrogel network (Figure 1b). In 2-step gelMA-Au hydrogels, chemical-coupling of AuCOOH NPs to gelMA macromolecules prior to photocrosslinking not only disrupted the gelMA hydrogel network but also likely decreased the crosslinking density of gelMA-Au macromolecules compared with gelMA macromolecules (Figure 1c).

2.3.2. Mechanical Properties—The compressive modulus of gelMA-Au hydrogels was measured and compared to gelMA alone before (day 0) and after 33 days of hydrolysis in Dulbecco's PBS (DPBS) to evaluate the hydrogel crosslinking density and hydrolytic stability. The compressive modulus of gelMA and gelMA-Au hydrogels was not statistically different ($p > 0.41$, ANOVA) at day 0 (Figure 3c). However, following 33 days of hydrolysis, the compressive modulus of 1-step gelMA-Au hydrogels was maintained at a similar level as day 0, but greater ($p < 0.01$, Tukey) than that for gelMA, gelMA+Au, and 2-step gelMA-Au hydrogels (Figure 3c). Taken together, these results suggest that 1-step gelMA-Au hydrogels prepared with AuMA NPs did not disrupt the initial mechanical properties of gelMA hydrogels and were more resistant to hydrolytic degradation. Additionally, physically-mixed gelMA+Au hydrogels and 2-step gelMA-Au hydrogels exhibited a greater effective swelling ratio (Figure 3b) but unchanged compressive modulus (Figure 3c) compared with gelMA alone. These results suggest that the Au NPs provided mechanical reinforcement that compensated for a disrupted hydrogel network and/or reduced crosslinking density. Supporting this observation, physically-entrapped gelMA+Au hydrogels were previously shown to exhibit a decreased swelling ratio and increased compressive modulus with increased concentration of Au nanorods.[37]

The hydrolytic stability of gelMA-Au NP hydrogels was also monitored longitudinally by contrast-enhanced micro-CT, inductively-coupled plasma optical emission spectroscopy (ICP-OES), and gravimetric analysis. All gelMA and gelMA-Au NP hydrogels were stable against hydrolysis for at least one month (Figure S4). Differences in the cumulative degradation between gelMA and gelMA-Au NP hydrogels after 30 days hydrolysis were not statistically significant ($p > 0.62$, ANOVA). However, the cumulative degradation measured by gravimetric analysis was greater than that measured by micro-CT and ICP-OES. For example, gelMA-Au hydrogels prepared by 1-step photocrosslinking with AuMA NPs exhibited a cumulative degradation of ~5% as measured by micro-CT and ICP-OES, and ~20% as measured by gravimetric analysis, after 30 days hydrolysis (Figure S4). The greater degradation measured by gravimetric analysis occurred nearly entirely within the first three days and was unchanged thereafter. The initial ~15% loss of mass within the first three days (Figure S4d) was not accompanied by release of Au NPs (Figure S4c). Taken together, these results suggest that gelMA and gelMA-Au NP hydrogels exhibited thermally-induced

deswelling upon incubation at 37°C[51] which caused an initial loss of mass as hydrogels re-equilibrated, and not hydrolytic degradation.

2.4. Longitudinal Monitoring of GelMA-Au NP Hydrogels During Enzymatic Degradation

Enzymatic degradation of gelMA-Au NP hydrogels was monitored longitudinally *in vitro* for more than three weeks by contrast-enhanced micro-CT and compared with concurrent measurements by gravimetric analysis and optical spectroscopy (Figure 4). Segmented micro-CT image reconstructions showed clear and repeatable changes in the hydrogel volume over time due to enzymatic degradation (Figure 4a). Importantly, contrast-enhanced micro-CT was able to quantitatively measure the degradation kinetics and differences in the degradation kinetics between 1-step gelMA-Au, physically-mixed gelMA+Au NP, and 2-step gelMA-Au hydrogels (Figure 4b, Table 1). The degradation kinetics measured by contrast-enhanced micro-CT (Figure 4b) exhibited close agreement with that measured by ICP-OES (Figure 4c) and gravimetric analysis (Figure 4d). Direct comparison of the degradation kinetics of 1-step gelMA-Au hydrogels measured by each technique (Figure 4e) revealed that the degradation kinetics measured by contrast-enhanced micro-CT were strongly correlated ($r > 0.96$, Pearson) with that measured by ICP-OES and gravimetric analysis. These results demonstrate the feasibility of contrast-enhanced micro-CT for non-invasive monitoring of gelMA-Au NP hydrogel degradation.

1-step gelMA-Au hydrogels exhibited slower degradation kinetics, while 2-step gelMA-Au hydrogels exhibited more rapid degradation kinetics, compared with gelMA and gelMA+Au hydrogels (Figure 4, Table 1). The slower degradation kinetics exhibited by 1-step gelMA-Au hydrogels was most likely the result of AuMA NPs participating in photocrosslinking to form additional crosslinks within the hydrogel network (Figure 1a). A common limitation of hydrogels is rapid degradation and/or burst release of encapsulated drugs.[39,52,53] Therefore, these results suggest that this limitation can be mitigated by incorporating AuMA NPs in photocrosslinked hydrogels. In contrast, the more rapid degradation kinetics exhibited by 2-step gelMA-Au hydrogels was most likely the result of Au NPs covalently-linked to gelMA molecules prior to photocrosslinking disrupting the hydrogel network and reducing the crosslinking density during photocrosslinking (Figure 1c), consistent with results for the effective swelling ratio and mechanical properties (Figure 3b,c).

Gravimetric measurements exhibited more rapid degradation at early time points than concurrent measurements by contrast-enhanced micro-CT and ICP-OES (Figure 4b–d). For example, the cumulative degradation of 1-step gelMA-Au hydrogels measured by gravimetric analysis was greater than that measured by contrast-enhanced micro-CT and ICP-OES at days 2–8 ($p < 0.05$, Tukey) while differences between micro-CT and ICP-OES were not statistically significant at any time point (Figure 4e). These differences were reflected in measurements of the degradation half-life (t_{50}) and rate (H) (Table 1). Gravimetric analysis cannot distinguish mass lost due to deswelling versus degradation of the hydrogel network. Therefore, these results suggest that measurements by contrast-enhanced micro-CT and ICP-OES more likely reflected the true degradation kinetics. The close agreement between micro-CT and ICP-OES further suggests that contrast-

enhanced micro-CT enabled precise and accurate measurement of hydrogel degradation non-invasively.

2.6. 3D Bioprinting GelMA Bioinks with AuMA NPs

GelMA bioinks supplemented with AuMA NPs were printed by extrusion (Figure 5a, S5a) and digital light processing (DLP) (Figure 5b, S5a) bioprinting. As noted above, gelMA prepolymer solutions supplemented with AuMA NPs exhibited similar rheological properties as gelMA alone (Figure S2) and shear-thinning behavior under flow, which is advantageous for high-fidelity extrusion bioprinting.[1,54]

2.6.1. Printing Fidelity—Two-layer lattice (Figure 5a) and cubic (Figure S5a) scaffolds were printed by air extrusion with adequate reproducibility in correspondence to the computer-aided design (CAD) models. The microscale printing fidelity of two-layer lattice scaffolds was quantified by the ratio of printed construct dimensions relative to the CAD model. Overall, the printing fidelity of 1-step gelMA-Au hydrogels was comparable to that of gelMA alone with only small differences in the strand angle and diameter (Figure 5c). Differences in the strand angle and uniformity between printed constructs and the CAD model were not statistically significant for both gelMA and 1-step gelMA-Au hydrogels. Differences in the interstrand area and strand diameter between printed constructs and the CAD model were most likely caused by viscoelastic flow after printing (creep) and die swell during extrusion (stress relaxation), respectively.[1,55] More complex constructs, including 10-layer lattice (Figure 5a) and hollow cylinder (Figure S5a) scaffolds, were also printed by embedded extrusion, which was previously shown to enable improved printing fidelity compared with air extrusion printing.[1]

DLP bioprinting was utilized to print 1-step gelMA-Au hydrogel constructs of varying 3D geometry, including a University of Notre Dame logo (Figure 5b), cylindrical tubes mimicking blood vessels (Figure 5b), and a cubic structure (Figure S5a). The macroscale printing fidelity of cylindrical tubes was quantified by the ratio of printed construct dimensions relative to the CAD model. Differences in the outer diameter between printed constructs and the CAD model were not statistically significant (Figure 5d). Differences in the inner diameter and corresponding wall thickness between printed constructs and the CAD model ($p < 0.005$, exact t-test) were most likely due to incomplete photocrosslinking caused by the absorption and scattering of light by Au NPs in the thick cross-section. Thus, further optimization of printing and photocrosslinking parameters is required. Nonetheless, for both extrusion and DLP bioprinting, dimensional differences between constructs and CAD models were consistent and can therefore be compensated by scaling dimensions in STL files.[56] Overall, gelMA bioinks supplemented with AuMA NPs exhibited suitable printability and dimensional fidelity.

2.6.2. Contrast-enhanced micro-CT.—Segmented micro-CT image reconstructions of the 10-layer lattice (Figure 5a) and cylindrical tube (Figure 5b) scaffolds demonstrated feasibility of non-invasive radiographic imaging of bioprinted constructs. AuMA NPs provided sufficient X-ray contrast for imaging both the macrostructure and microstructural features, whereas constructs printed from gelMA alone could not be imaged by micro-CT.

2.6.3. Mechanical properties.—The mechanical integrity of gelMA and gelMA-Au hydrogels printed by air extrusion was evaluated on cubic constructs in unconfined uniaxial compression and microindentation after reaching equilibrium swelling (Figure S5). Differences in the compressive modulus and indentation modulus between gelMA and 1-step gelMA-Au hydrogels were not statistically significant. Therefore, AuMA NPs did not disrupt the mechanical properties of bioprinted 1-step gelMA-Au hydrogels, consistent with measurements for molded 1-step gelMA-Au hydrogels (Figure 3c).

2.7. Cell Viability in Bioprinted GelMA-Au NP Hydrogels

Cell viability in 1-step gelMA-Au hydrogels was assessed by both 2D and 3D culture of human umbilical vein endothelial cells (HUVECs) in bioprinted constructs (Figure 6). In 2D culture, over 95% of cells seeded onto the surface of 1-step gelMA-Au hydrogel substrates remained viable at days 1 and 7. In 3D culture, over 70% of cells that were encapsulated in the bioink before printing remained viable within 1-step gelMA-Au hydrogels at days 1 and 7. The level of cell viability in 3D culture was consistent with previous studies for gelMA alone at comparable gelMA concentration and photocrosslinking parameters.[57–60] Decreased cell viability in 3D culture is commonly observed in bioprinted constructs due to cellular damage caused by mechanical forces introduced to cells during extrusion and/or UV light exposure during crosslinking.[54,60,61] Printing-induced damage to cells can be reduced using a lower printing pressure or speed, larger gauge syringe needle, or lower UV intensity or exposure time. Limited nutrient transport in 3D culture, especially hydrogels prepared with high gelMA concentration, may have also contributed to decreased cell viability.[61] Importantly, however, there was no loss of viability between days 1 and 7 ($p > 0.71$, ANOVA) in either 2D or 3D culture. Moreover, HUVECs exhibited a more elongated and mature morphology at day 7 compared with day 1 in both 2D and 3D culture. Taken together, these results suggest that 1-step gelMA-Au hydrogels are cytocompatible with endothelial cells.

2.8. Application of AuMA NPs to Other Photopolymerized Hydrogels

HAMA-Au hydrogels were also prepared with AuMA NPs by one-step photocrosslinking to demonstrate the use of AuMA NPs in other photocrosslinkable hydrogels. The effective swelling ratio of as-prepared HAMA-Au hydrogels was increased compared with HAMA alone ($p < 0.05$, Tukey) (Figure S6a). This result suggests that, unlike in gelMA hydrogels, AuMA NPs decreased the crosslinking density of HAMA hydrogels, most likely due to the lower methacrylation degree of HAMA (20–50%) versus gelMA (80%) in this study. The compressive modulus of HAMA and HAMA-Au hydrogels was not significantly different ($p > 0.75$, ANOVA) (Figure S6b). This result suggests that the Au NPs provided mechanical reinforcement that compensated for the reduced crosslinking density, which is consistent with the results for gelMA-Au hydrogels (Figure 3b,c). Both HAMA and 1-step HAMA-Au hydrogels were stable against hydrolysis for at least four weeks (Figure S6c–f). Differences in the cumulative degradation between HAMA and 1-step HAMA-Au hydrogels were not statistically significant (Figure S6f). Differences in the cumulative degradation of 1-step HAMA-Au hydrogels measured by contrast-enhanced micro-CT, ICP-OES, and gravimetric analysis were also not statistically significant. Taken together, these results suggest that HAMA and other methacrylate-modified hydrogels are also readily prepared with AuMA

NPs by one-step photocrosslinking to enable non-invasive monitoring by contrast-enhanced micro-CT.

2.9. Study Implications and Limitations

A one-step photocrosslinking strategy (Figure 1) was introduced for preparing bioprinted constructs with hybrid hydrogel-NP bioinks. For proof-of-concept, methacrylate-modified NPs (AuMA NPs) were prepared (Figure 2) and covalently-linked to gelMA and HAMA in one-step during photocrosslinking. Importantly, the approach can be readily extended to other methacrylate-modified NP and hydrogel compositions. The one-step photocrosslinking strategy combined the advantages of both chemical coupling and physical mixing; NPs were able to be covalently-linked to the hydrogel network by photocrosslinking after being directly added to a prepolymer solution (Figure 1). Prior to this study, Au NPs had only been physically-entrapped within gelMA hydrogels without chemical coupling.[36–38,54] The immobilization of NPs by covalent linking to the hydrogel network is beneficial for minimizing disruption of the hydrogel structure and properties (Figure 3), enabling accurate and reliable monitoring of NP release and hydrogel degradation (Figure 4), facilitating 3D bioprinting of CT-visible hydrogel constructs (Figure 5), and reducing the risk of cytotoxicity due to uncontrolled (burst) release of NPs (Figure 6).

Au NPs were advantageous due to facile surface modification and strong X-ray attenuation, but strong absorption and scattering of UV and visible light inhibited photocrosslinking and the concentration of Au NPs that could be incorporated into hydrogels. Therefore, other NP compositions may yet prove to be advantageous in enabling the use of higher NP concentrations for X-ray contrast or other functionalities, but with less detrimental effect on photocrosslinking. Furthermore, the concentration of methacrylate-modified NPs and/or the density of methacrylate ligands on NPs may offer an ability to tailor the photocrosslinked hydrogel crosslinking density and degradation/release rate.

GelMA-Au hydrogels prepared by one-step photocrosslinking with 10 mM AuMA NPs provided little or no disruption of the hydrogel structure and properties (Figure 3), ample X-ray contrast for accurate monitoring of degradation/release (Figure 4), high fidelity imaging of 3D bioprinted scaffolds (Figure 5), and suitable cytocompatibility (Figure 6). Previous studies investigating *in vitro* and *in vivo* micro-CT imaging and monitoring degradation of hydrogel or polymeric scaffolds have generally used greater contrast agent concentrations, including 100 mM Gd_2O_3 NPs,[28] 80 mM (~13.6 wt%) Au NPs,[29] 20 wt% Au NPs,[62] 100 mg/mL iohexol (~365 mM iodine),[30] and 11.4 wt% (~500 mM) iodine.[63] Of particular note, 50 mM TaO_x NPs were reported to provide sufficient signal/noise within tissue phantoms for clinical CT imaging.[64] On the other hand, another study reported *in vivo* micro-CT imaging of 3D-printed gelMA+Au scaffolds comprising 0.16 mM Au NPs,[38] but did not report X-ray attenuation in HU making interpretation difficult. Therefore, the relatively low concentration of Au NPs required for sufficient CT imaging contrast and monitoring degradation of the scaffolds in this *in vitro* study is encouraging but must be further investigated *in vivo*.

The opportunity to utilize CT for noninvasive, longitudinal, and volumetric monitoring of scaffolds is tempered by a need for greater contrast agent concentrations compared to other

imaging modalities. MRI is able to provide sufficient contrast for imaging and monitoring degradation in hydrogel or polymeric scaffolds at lower NP concentrations, e.g., ~0.4–10 mM (~0.01–0.2 wt%) Fe_3O_4 NPs.[25–27,64] However, MRI is limited by low spatial and temporal resolution.[13] Optical imaging (e.g., fluorescence) has been more widely used to image and monitor scaffolds with even lower concentrations (μM) of fluorophores or NPs,[19–24] but is not suitable for deep tissue imaging due to the limited depth of light penetration(<1 cm).[65] Therefore, the opportunity to leverage CT for deep tissue imaging at high spatial and temporal resolution is dependent on the minimum effective vs. maximum safe contrast agent concentration for imaging.

GelMA-Au hydrogels prepared by one-step photocrosslinking were shown to be cytocompatible with endothelial cells in 2D culture and were no less cytocompatible than gelMA alone in 3D culture. Previous studies investigating gelMA+Au hydrogels reported either similar cell viability under similar conditions as this study,[54] enhanced cell activity at lower or similar concentrations of Au NPs,[36,37] and decreased cell viability at much lower concentrations of Au NPs.[38] Therefore, the safety of gelMA-Au hydrogels prepared by one-step photocrosslinking is promising but requires further investigation, including cytotoxicity in 3D culture and the *in vivo* toxicity, biodistribution, and clearance of released NPs.

3. Conclusions

Methacrylate-modified gold nanoparticles (AuMA NPs) were prepared and covalently-linked to methacrylate-modified hydrogels (gelMA and HAMA) in one-step during photocrosslinking. Photopolymerized hydrogels exhibited a linear increase in X-ray attenuation with increased Au NP concentration to enable quantitative imaging by contrast-enhanced micro-CT. The hydrolytic and enzymatic degradation kinetics of gelMA-Au NP hydrogels were longitudinally monitored by micro-CT for up to one month *in vitro*, and were consistent with concurrent measurements by gravimetric analysis and optical spectroscopy. Importantly, AuMA NPs provided little or no disruption to the hydrogel network, rheology, mechanical properties, and hydrolytic stability compared with gelMA alone. GelMA-Au NP hydrogels were able to be printed into well-defined 3D architectures supporting endothelial cell viability. Thus, AuMA NPs enabled the preparation of photopolymerized hydrogels and bioprinted scaffolds with tunable X-ray contrast for noninvasive, longitudinal monitoring of degradation and NP release by micro-CT.

4. Experimental Section

Synthesis of AuCOOH NPs:

AuCOOH NPs were synthesized by surface functionalizing bare Au NPs, ~12 nm in diameter prepared by the citrate reduction method, with mercaptosuccinic acid (MSA).[29,44] Briefly, 0.1 g gold (III) chloride trihydrate ($HAuCl_4 \cdot 3H_2O$, 99.9%, Sigma-Aldrich) was added to 500 mL deionized (DI) water and heated to boiling while stirring. Once boiling, 0.5 g trisodium citrate dihydrate ($C_6H_5Na_3O_7 \cdot 2H_2O$, ACS reagent, Sigma-Aldrich) was added to the mixture. The mixture was boiled for another 20 min, cooled to room temperature and stirred overnight. As-prepared Au NPs were collected in a volumetric flask and titrated

to 500 mL. An aqueous solution containing 15 mL of 10 mM MSA ($C_4H_6O_4S$, 97%, Sigma-Aldrich) was added to the Au NP solution and stirred overnight. As-prepared AuCOOH NPs were collected by centrifugation (Sorvall RC-6 Plus, Thermo Scientific) at ~11,000*g* for 1 h and thrice washed with DI water. The final AuCOOH NP stock solution was concentrated to 94 mM as verified by inductively-coupled plasma optical emission spectroscopy (ICP-OES).

Synthesis of AuMA NPs:

AuMA NPs were synthesized by covalently-linking AuCOOH NPs with 2-aminoethyl methacrylate (AEMA, 90%, $C_6H_{11}NO_2$·HCl, Sigma-Aldrich) using carbodiimide/succinimide chemistry (Figure 2a). First, 0.5 mmol AuCOOH NPs were added to 200 mL ethanol (80% v/v) containing 1.44 g 1-ethyl-3-(3-dimethylaminopropyl) carbodiimide hydrochloride (EDC, Sigma-Aldrich) and 0.65 g *N*-hydroxysulfosuccinimide (NHS, Sigma-Aldrich), which was then mixed with another 200 mL ethanol (80% v/v) containing 0.495 g fully dissolved AEMA, such that the molar ratio of Au:EDC:NHS:AEMA was 1:15:6:6. The mixture was vigorously stirred under nitrogen protection for 24 h at room temperature to obtain AuMA NPs. AuMA NPs were also prepared with a higher degree of methacrylation (Au:EDC:NHS:AEMA = 1:75:30:30) but exhibited strong hydrophobicity and were not utilized further. After the reaction, AuMA NPs were collected by centrifugation at 8400*g* for 30 min and washed thrice with DI water. The final AuMA NP stock solution was concentrated to 90 mM as verified by ICP-OES.

ICP-OES:

The concentration of as-prepared AuCOOH NPs and AuMA NPs, as well as the concentration of Au NPs released from hydrogels into supernatant media during *in vitro* hydrolytic and enzymatic degradation, was measured using ICP-OES. As-prepared or supernatant Au NP solutions were digested in 5% aqua regia before analysis. Calibration curves were established by diluting certified standard Au solutions (Assurance Grade, SPEX CertiPrep).

Transmission Electron Microscopy (TEM):

The size and morphology of as-prepared AuCOOH and AuMA NPs were characterized by TEM (JEOL 2011, JEOL) at an accelerating voltage of 120 kV. Specimens were prepared by pipetting 10 μL of as-prepared NPs onto carbon-coated grids and evaporating the solvent in an oven at 60°C. The mean (± standard deviation) diameter and size distribution were measured from at least 100 NPs sampled from digital images at 120,000X magnification (ImageJ v1.51).

Dynamic Light Scattering (DLS):

The hydrodynamic particle diameter and zeta potential of as-prepared AuCOOH and AuMA NPs were measured by DLS (Zetasizer ZS90, Malvern Instruments) at 25°C. Specimens were prepared by dispersing NPs in DI water at 0.5 mM and 5 mM concentration for hydrodynamic diameter and zeta potential measurements, respectively. The mean (± standard deviation) hydrodynamic diameter and zeta potential were measured from three sample replicates.

The long-term colloidal stability of AuMA NPs was monitored for up to 40 d by longitudinal measurements of the hydrodynamic particle diameter and polydispersity index (PDI) using DLS. A stock solution of AuMA NPs was prepared at 12 mM concentration in DI water and stored at 4°C protected from light. At each time point, aliquots were diluted to 0.6 mM concentration and warmed to 25°C. Aliquots were dispersed by either vortexing for 40 s or ultrasonication for 40 s at 20% amplitude pulsed for 1 s on and 0.5 s off (model 500, Fisher Scientific). The mean (± standard deviation) hydrodynamic diameter and PDI were measured for each time point from three replicates for vortexed samples. One sample was measured for each time point for ultrasonication.

Fourier Transform Infrared Spectroscopy (FTIR):

Methacrylate surface functionalization of as-prepared AuMA NPs was verified by FTIR transmission spectra of AEMA powder and lyophilized AuMA NPs acquired using an attenuated total reflection (ATR) module (Tenor 27, Bruker) as an average of 64 scans over 4000–400 cm^{-1} at room temperature.

Nuclear Magnetic Resonance (NMR):

Methacrylate surface functionalization of as-prepared AuMA NPs was also characterized by ^{1}H NMR spectra of AEMA powder and lyophilized AuMA NPs acquired at 25°C on a spectrometer (AVANCE III HD 500, Bruker) with 8012.8 Hz spectral width, 4.0 s acquisition time, 6.5 ms pulse, and referenced to the solvent peak of deuterium oxide (D_2O) at 4.79 ppm. Specimens were prepared by dissolving AEMA powder and lyophilized AuMA NPs in 0.6 mL of D_2O (Sigma-Aldrich) at a concentration of 10 and 30 mg/mL, respectively.

GelMA Preparation:

GelMA with a degree of functionalization (DoF) >75–80% was prepared using previously established methods.[66,67] Briefly, 8 g porcine gelatin (Sigma) was dissolved in 100 mL phosphate-buffered saline (PBS) at 50°C under stirring, followed by the dropwise addition of 8 mL methacrylic anhydride (MAA, Sigma) which was maintained at 50°C under stirring for 3 h. The gelMA solution was then centrifuged to remove impurities, diluted with 100–200 mL PBS, and dialyzed for 7 d to remove unreacted MAA, lyophilized, and stored away from light at −20°C until further use. Lyophilized gelMA powder was reconstituted in PBS at 40% w/v and heating to 60°C for the preparation of prepolymer solutions.

GelMA and GelMA-Au NP Prepolymer Solutions:

All gelMA and gelMA-Au NP prepolymer solutions were prepared with 10 or 20% w/v gelMA and up to 37 mM Au NPs. Prepolymer solutions for one-step photopolymerized gelMA-Au NP hydrogels (1-step gelMA-Au) and physically-mixed gelMA+Au NP hydrogels (gelMA+Au) were prepared by mixing appropriate volumes of the gelMA prepolymer solution with AuMA or AuCOOH NPs, respectively, at 60°C and vortexing for 2 min. Prepolymer solutions for gelMA-Au NP hydrogels prepared by two-step chemical-coupling and photocrosslinking (2-step gelMA-Au) were prepared by covalently-linking gelMA and AuCOOH NPs via EDC/NHS chemistry prior to photocrosslinking. Appropriate volumes of the gelMA prepolymer solution were mixed with AuCOOH NPs at 60°C and

vortexed for 2 min. The mixture was loaded into a 4.78 mm inner diameter mold, cooled to 4°C to induce thermal gelation, removed from the mold, and sectioned into cylindrical specimens, 5.0 mm in height, using a razor blade. Specimens were then soaked in 30 mL ethanol (80% v/v) containing EDC and NHS at 4°C with a Au:EDC:NHS molar ratio of 1:1:1 for 18 h. A higher Au:EDC:NHS molar ratio (Au:EDC:NHS = 1:160:64 for 6 h) was also investigated but compromised the thermal sol-gel transition and was not utilized further. After the reaction, specimens were thrice washed with DI water and heated above 60°C to obtain a chemically-coupled gelMA-Au NP prepolymer solution.

Rheological Properties:

GelMA and gelMA-Au NP prepolymer solutions comprising 20% w/v gelMA and 10 mM Au NPs were characterized by loading 700 μL into the parallel plates (8 mm diameter, 1000 μm gap) of a rheometer (Discovery HR-2, TA Instruments). Storage moduli (G') and loss moduli (G'') were measured at a constant frequency (1 Hz) and strain amplitude (1%) over a temperature sweep from 37 to 5°C at a cooling rate of 3°C/min. The flow behavior of prepolymer solutions was also measured over a steady state strain rate sweep from 0.1 to 100 s^{1} at 25°C. Three sample replicates were measured for each test and group.

Photocrosslinking:

GelMA and gelMA-Au NP prepolymer solutions comprising 10 or 20% w/v gelMA and up to 37 mM Au NPs were supplemented with 0.5–1.0% w/v 2-hydroxy-4′-(2-hydroxyethoxy)-2-methylpropiophenone (Irgacure 2959, Sigma-Aldrich) or lithium phenyl-2,4,6-trimethylbenzoylphosphinate (LAP, Allevi) photoinitiator and incubated for 1 h, 24 h, or 7 d at 4°C. Prepolymer solutions with photoinitiator were loaded into cylindrical molds (4.78 mm inner diameter, 3 mm height) and photocrosslinked under an ultra-violet (UV) light source (OmniCure S1500, 320–390 nm) at 7, 15 or 30 mW/cm^2 for 4–6 min at ambient temperature. After initial investigations to optimize the above photocrosslinking parameters, all gelMA and gelMA-Au NP hydrogels were prepared with 20% w/v gelMA and up to 37 mM Au NPs by incubating prepolymer solutions with 0.5% w/v LAP photoinitiator for 24 h at 4°C and photocrosslinking under UV irradiation at 30 mW/cm^2 for 4 min.

Photocrosslinking of gelMA and AuMA NPs was verified by a surface photocrosslinking experiment between gelMA and AuMA NPs, as well as gelMA and AuCOOH NPs as a negative control. Thin layers of gelMA were formed on glass slides by depositing 50 μL of 20% w/v gelMA with 0.5% w/v LAP photoinitiator. After gelMA layers were solidified at ambient temperature, 30 μL aliquots of 60 mM AuMA NPs or AuCOOH NPs were deposited on top of the gelMA layers. GelMA-Au NP bilayers were then photocrosslinked under UV irradiation at 30 mW/cm^2 for 4 min. After photocrosslinking, bilayers were washed with DI water to remove unreacted AuMA or AuCOOH NPs from the gelMA surface. The surface of gelMA layers was imaged by stereomicroscopy (SMZ800, Nikon) and reflected light microscopy (ME600, Nikon). The attachment of Au NPs to the gelMA surface was measured as the percent surface area coverage in representative segmented images (ImageJ).

Contrast-Enhanced Micro-CT:

The X-ray attenuation of gelMA-Au NP hydrogels was measured by micro-CT (μCT-80, Scanco Medical AG) for as-prepared gelMA-Au NP hydrogels comprising 20% w/v gelMA and 0–37 mM Au NPs. PBS and rat myocardium were imaged as soft tissue controls. Micro-CT images were also acquired for longitudinal measurements of degradation in gelMA-Au NP hydrogels initially containing 10 mM Au NPs and 3D bioprinted gelMA-Au NP constructs. Micro-CT images were acquired at 70 kVp tube potential, 144 μA beam current, and 0.5 mm Al beam filtration with 125 projections at 800 ms integration time. Noise in grayscale images was reduced using a Gaussian filter (sigma = 0.8, support = 1). 3D images were reconstructed with a 100 μm isotropic voxel size chosen to replicate *in vivo* imaging methods. The linear X-ray attenuation (cm^{-1}) was measured within a volume of interest (VOI) and converted to Hounsfield units (HU) using internal calibration to air and water as −1000 and 0 HU, respectively. The VOI included the entire hydrogel volume for as-prepared gelMA-Au NP hydrogels or the entire volume of the media within Eppendorf tubes for longitudinal measurements of gelMA-Au NP hydrogel degradation. The total volume of the hydrogel and/or hydrogel fragments was segmented from the media using a fixed global threshold of 64, which corresponded to a linear attenuation of 0.51 cm^{-1} or 61 HU. Three sample replicates were imaged for each Au NP concentration in as-prepared gelMA-Au NP hydrogels. Five sample replicates were imaged longitudinally for each group during degradation of gelMA-Au NP hydrogels.

Swelling Ratio:

The effective swelling ratio of gelMA and gelMA-Au NP hydrogels comprising 20% w/v gelMA and 10 mM Au NPs was measured by gravimetric analysis.[3,49,68] Hydrogels were incubated in Dulbecco's PBS (DPBS, Sigma-Aldrich) at 37°C for 24 h to reach the equilibrium swelling. The effective swelling ratio was measured by the total mass change after 24 h equilibrium relative to the initial mass. Ten sample replicates were measured for each group.

Compression Testing:

GelMA and gelMA-Au NP hydrogels comprising 20% w/v gelMA and 10 mM Au NPs were loaded in unconfined uniaxial compression to 80% strain at a displacement rate of 0.05 mm/s using an electromagnetic test instrument (ElectroForce 3220, Bose). Hydrogels were incubated in DPBS for 24 h to reach equilibrium swelling prior to testing; specimens measured ~4 mm in diameter and ~3 mm in height. Load and displacement data were collected at a sampling rate of 10 Hz using a 25 lb load cell (MBP, Interface) and linear variable displacement transducer, respectively. The compressive modulus was calculated as the slope of the stress–strain curve over 10–20% strain using linear least squares regression ($R^2 > 0.95$). At least three and at most five sample replicates were tested for each group.

In Vitro Hydrolytic and Enzymatic Degradation:

GelMA and gelMA-Au NP hydrogels comprising 20% w/v gelMA and 10 mM Au NPs were evaluated using *in vitro* models of hydrolytic and enzymatic degradation.[29] Hydrogels were incubated in DPBS for 24 h prior to degradation to establish the day 0 time point.

Hydrogels were subsequently placed in Eppendorf tubes containing 0.2 mL DPBS for hydrolysis or 0.02 mg/mL bacterial (*Clostridium histolyticum*) collagenase (Collagenase B, Roche) in 0.2 mL DPBS for enzymolysis, and incubated at 37°C. Hydrolytic and enzymatic degradation were measured longitudinally at 24 h time points for up to one month. At each time point, the supernatant media was separated from hydrogels and/or hydrogel fragments by centrifugation at 500*g* for 1 min and the concentration of released Au NPs was measured by ICP-OES as described above, such that degradation was measured spectroscopically by the cumulative amount of Au released into the media relative to the total amount in as-prepared gelMA-Au NP hydrogels. The remaining hydrogels and/or hydrogel fragments were then weighed on a mass balance, such that degradation was also measured gravimetrically by the total mass change relative to the initial hydrogel mass on day 0. Next, 50 μL DPBS was added to the tube and the hydrogel was imaged by micro-CT, as described above, such that degradation was also measured radiographically by the difference in segmented scaffold volume relative to the initial scaffold volume. Finally, additional fresh DPBS and/or enzyme solution was added back to the tube for continued hydrolytic or enzymatic degradation. Five sample replicates were measured longitudinally for each group.

Enzymatic degradation kinetics were modeled by non-linear lest squares regression using a four-parameter logistic model (GraphPad Prism 9) forcing the *y*-axis from 0 to 100% as,

$$y = \frac{100}{1 + 10^{H \cdot (t_{50} - t)}} \quad (1)$$

where y is the scaffold degradation (%), t is time (days), t_{50} is the degradation half-life (days), and H is the Hill slope or steepness of the kinetic curves which can be used to describe the hydrogel degradation rate. The degradation half-life, Hill slope, and 95% confidence interval were determined from the model. The correlation coefficient (R^2) was greater than 0.9 for each group.

Hydrolytic degradation kinetics measured by micro-CT and ICP-OES were modeled by linear least squares regression (JMP 16). Hydrolytic degradation kinetics measured by gravimetrical analysis were modeled by non-linear least squares regression (GraphPad Prism 9) using the four-parameter logistic model (Equation 1) with a log-transform of time.

3D Bioprinting Bioinks:

Bioinks were prepared with gelMA and one-step photopolymerized gelMA-Au NP prepolymer solutions comprising 20% w/v gelMA, 10 mM AuMA NPs, and 0.5% w/v LAP photoinitiator using methods described above.

Air Extrusion Bioprinting:

Cubic ($5 \times 5 \times 2.5$ mm^3) and two-layer lattice scaffolds with a crosshatch pattern (1 mm^2 area, 0.3 mm line width, 9 mm strand segment length, and 60° interstrand angle) were printed using a microextrusion bioprinter (BioAssemblyBot, Advanced Solutions Life Sciences). GelMA or gelMA-Au NP inks were loaded in the printing syringe with a 27-gauge tapered needle and printed at room temperature, 6.5 mm/s printing speed, and 0.25

mm line height. Once printed, constructs were immediately photocrosslinked under UV light at 30 mW/cm^2 for 4 min and subsequently washed with PBS before further evaluation.

Embedded Extrusion Bioprinting:

A 10-layer lattice scaffold (10 × 10 × 2 mm^3) and hollow cylinder scaffold (6.4 mm outer diameter, 4 mm inner diameter, 2.5 mm in height) were designed and prepared by embedded bioprinting using a microextrusion bioprinter (BioX, CELLINK).[1] The embedding (support) bath was prepared using 0.4% w/v Carbopol (ETD 2020, Lubrizol) dissolved in DI water. GelMA-Au NP inks were loaded in the printing syringe with a 27-gauge steel needle with a length of 0.5 in and printed at room temperature, 30 kPa printing pressure, and 10 mm/s printing speed. Once printed, constructs were immediately photocrosslinked under UV light at 30 mW/cm^2 for 3 min and subsequently washed by PBS for 10 min before further evaluation.

Digital Light Processing (DLP) Bioprinting:

Three distinct geometric models were created using Fusion360 (Autodesk) and Blender 2.91 (Blender Foundation). These included a cylindrical tube (3 mm outer diameter, 1.5 mm inner diameter), a cube (5 × 5 × 5 mm^3), and a more complex 3D model of the University of Notre Dame (ND) logo. STL files for each model were processed printed using a DLP bioprinter (Lumen X, CELLINK) with a 0.1 mm layer height, 67% projector power at 10 s/layer (~25 mW/cm^2), and 2X burn-in on the initial layers.

Printing Fidelity:

Macroscopic and microscopic (strand-level) dimensional fidelity was assessed on cylindrical tubes and two-layer lattice scaffolds prepared by DLP bioprinting and air extrusion bioprinting, respectively. Construct dimensions measured on digitized optical microscopy images via ImageJ were compared with reference values in the computer-aided design (CAD) model as a ratio, such that a ratio of 1 indicated no deviation. Macroscopic measurements of the cylindrical tube wall thickness ratio, outer diameter ratio, and inner diameter ratio were taken from nine sample replicates. Microscopic measurements of the lattice scaffold strand angle ratio, interstrand area ratio, strand diameter ratio, and strand uniformity ratio[1] were taken from five sample replicates.

Mechanical Properties:

Macroscopic and microscopic (strand-level) mechanical properties of cubic gelMA and gelMA-Au NP scaffolds (5 × 5 × 2.5 mm^3) prepared by air-extrusion bioprinting were measured by unconfined uniaxial compression and microindentation, respectively. Scaffolds were loaded in unconfined uniaxial compression to 50% strain at a displacement rate of 0.02 mm/s using a micromechanical test instrument (Mach-1, Biomomentum). The compressive modulus was calculated as the slope of the stress–strain curve over 10–20% strain using linear least squares regression. For microindentation, scaffolds were loaded on the same instrument with a 500 μm diameter probe to a depth of 100 μm at a displacement rate of 2 μm/s. The reduced elastic modulus was calculated by the Oliver-Pharr method[69] using the unloading stiffness measured by linear lest squares regression from the initial 10–20% of the

unloading force-displacement curves. For each test, three gelMA sample replicates and four gelMA-Au NP sample replicates were measured for each group.

Cell viability in 2D and 3D Culture.

Human umbilical vein endothelial cells (HUVECs) were cultured in T75 flasks and maintained in complete HUVEC media (VascuLife VEGF Endothelial Medium Complete Kit) supplemented with 1% penicillin/streptomycin (Gibco). HUVEC media was changed every 3 days until cells reached 90% confluency. Cells were then passaged, evaluated, and used for cell culture experiments. For 2D cell culture, a 250 μL prepolymer solution was pipetted into 24-well plates and photocrosslinked under UV light at 10 mW/cm^2 for 1 min. HUVECs were seeded onto the surface of gelMA-Au NP substrates at 1×10^4 cells/well. After 1 h incubation, 1 mL of HUVEC media was added to each well for cell culture and changed every two days. For 3D cell culture, HUVECs were mixed in gelMA-Au NP inks at a density of 8×10^6 cells/mL. Lattice scaffolds ($10 \times 10 \times 0.2$ mm^3) were printed in an ultra-low attachment 6-well plate by embedded bioprinting using methods described above. Printed scaffolds were photocrosslinked under UV light at 10 mW/cm^2 for 1 min and immediately cultured in HUVEC media. Cell viability was measured by live/dead assay on days 1 and 7 post-seeding or post-printing. Fluorescent dyes, including 1 μg/mL calcein-AM and 20 μg/mL propidium iodide (Biotium) were added to the culture medium to selectively stain live (green) and dead (red) cells, respectively. After 20 min incubation, substrates or scaffolds were rinsed with fresh culture media and imaged by fluorescence microscopy (DFC3000 G, Leica). Three randomly-selected image fields were evaluated using ImageJ for each of three sample replicates at each time point.

HAMA and HAMA-Au NP Hydrogels:

HAMA and HAMA-Au NP hydrogels were prepared with AuMA NPs by one-step photocrosslinking to demonstrate the use of AuMA NPs in other photocrosslinkable hydrogels. HAMA with a DoF of 20–50% and molecular weight of 50,000–70,000 HAMA (Sigma-Aldrich) was dissolved in DPBS at 80°C to obtain a 10% w/v HAMA prepolymer solution. HAMA and HAMA-Au NP prepolymer solutions comprising 5% w/v HAMA, 10 mM AuMA NPs, and 0.5% w/v LAP photoinitiator were prepared by mixing the HAMA prepolymer solution with AuMA NPs, vortexing for 2 min, adding LAP, and incubating for 24 h at 4°C. Cylindrical hydrogels were prepared by loading the prepolymer solutions into molds (4.78 mm inner diameter, 3 mm height) and photocrosslinking under UV irradiation (320–390 nm) at 30 mW/cm^2 for 4 min.

The effective swelling ratio and compressive mechanical properties of HAMA and HAMA-Au NP hydrogels were measured using methods described above. At least four and at most seven sample replicates were tested for each measurement and group.

In vitro hydrolytic degradation of HAMA and HAMA-Au NP hydrogels were evaluated longitudinally by micro-CT, ICP-OES, and gravimetric analysis using methods described above, except that micro-CT and gravimetric degradation measurements were normalized by the day 1 time point instead of day 0 because equilibrium swelling was not reached until day 1. Hydrolytic degradation kinetics measured by micro-CT, ICP-OES and gravimetric

analysis were modeled by linear least squares regression (JMP 16). At least five and at most seven sample replicates were measured longitudinally for each group.

Statistical Analysis:

All quantitative measurements were reported as the mean (± standard deviation) of at least three replicates. Tukey outlier box plots were used to screen for possible outliers defined as data points located outside the interquartile range by more than 1.5-times the interquartile range; one data point was removed for the measured swelling ratio of gelMA hydrogels. The effect of the Au NP concentration on the gelMA-Au NP hydrogel X-ray attenuation was examined using linear least squares regression (JMP 16, SAS Institute). The effect of shear rate on the apparent viscosity of gelMA and gelMA-Au NP prepolymer solutions was also examined using linear least squares regression on a log transform of the data. Differences in the degradation kinetics of hydrogels measured by micro-CT, ICP-OES, and gravimetrical analysis were examined by multivariate linear correlation using Pearson's correlation coefficient (JMP 16). The effects of synthetic methods and/or hydrogel composition on the rheological properties, swelling ratio, mechanical properties, degradation kinetics, printing fidelity, and cell viability were examined by one-way analysis of variance (ANOVA) and analysis of covariance (ANCOVA). *Post hoc* comparisons were performed using Tukey's HSD test (JMP 16). Differences in measured printing fidelity ratios were also examined using an exact *t*-test with a hypothesized mean of 1. The level of significance for all tests was set at $p < 0.05$.

Supplementary Material

Refer to Web version on PubMed Central for supplementary material.

Acknowledgments

L.L. was supported by a Materials Science and Engineering Program Doctoral Fellowship from the University of Notre Dame. C.J.G was supported by a National Science Foundation (NSF) Graduate Research Fellowship (GE-1650044) and the American Heart Association (AHA) Predoctoral Fellowship (20PRE35080132). C.J.E. was supported by the Martell Family Ph.D. Fellowship at the University of Notre Dame. The authors acknowledge additional support from the Kelly Cares Foundation, National Institutes of Health (R00HL127295), Pediatric Research Alliance, and Emory University Dean's Imagine, Innovate and Impact (I3) Research Award. The authors acknowledge the Center for Environmental Science and Technology (CEST) for use of ICP-OES and FTIR, the Materials Characterization Facility (MCF) for rheometry, and Dr. Pinar Zorlutuna for providing the myocardial tissue sample, all from the University of Notre Dame.

Data Availability Statement

The data that support the findings of this study are available from the corresponding author upon reasonable request.

References

[1]. Ning L, Mehta R, Cao C, Theus A, Tomov M, Zhu N, Weeks ER, Bauser-Heaton H, Serpooshan V, ACS Appl. Mater. Interfaces 2020, 12, 44563. [PubMed: 32966746]

[2]. Kong B, Chen Y, Liu R, Liu X, Liu C, Shao Z, Xiong L, Liu X, Sun W, Mi S, Nat. Commun 2020, 11, 1435. [PubMed: 32188843]

[3]. Schuurman W, Levett PA, Pot MW, van Weeren PR, Dhert WJA, Hutmacher DW, Melchels FPW, Klein TJ, Macromol. Biosci 2013, 13, 551. [PubMed: 23420700]

[4]. Burdick JA, Prestwich GD, Adv. Mater 2011, 23, H41. [PubMed: 21394792]

[5]. Ifkovits JL, Tous E, Minakawa M, Morita M, Robb JD, Koomalsingh KJ, Gorman JH, Gorman RC, Burdick JA, Proc. Natl. Acad. Sci 2010, 107, 11507. [PubMed: 20534527]

[6]. Hjortnaes J, Camci-Unal G, Hutcheson JD, Jung SM, Schoen FJ, Kluin J, Aikawa E, Khademhosseini A, Adv. Healthc. Mater 2015, 4, 121. [PubMed: 24958085]

[7]. Nguyen T, Watkins KE, Kishore V, J. Biomed. Mater. Res. A 2019, 107, 1541. [PubMed: 30882990]

[8]. Drzewiecki KE, Malavade JN, Ahmed I, Lowe CJ, Shreiber DI, Technology 2017, 5, 185. [PubMed: 29541655]

[9]. Brinkman WT, Nagapudi K, Thomas BS, Chaikof EL, Biomacromolecules 2003, 4, 890. [PubMed: 12857069]

[10]. Nicol E, Biomacromolecules 2021, 22, 1325. [PubMed: 33793224]

[11]. Yu C, Schimelman J, Wang P, Miller KL, Ma X, You S, Guan J, Sun B, Zhu W, Chen S, Chem. Rev 2020, 120, 10695. [PubMed: 32323975]

[12]. Yue K, Santiago GT, Alvarez MM, Tamayol A, Annabi N, Khademhosseini A, Biomaterials 2015, 73, 254. [PubMed: 26414409]

[13]. Appel AA, Anastasio MA, Larson JC, Brey EM, Biomaterials 2013, 34, 6615. [PubMed: 23768903]

[14]. Nam SY, Ricles LM, Suggs LJ, Emelianov SY, Tissue Eng. B 2015, 21, 88.

[15]. Rice MA, Waters KR, Anseth KS, Acta Biomater. 2009, 5, 152. [PubMed: 18793879]

[16]. Gudur M, Rao RR, Hsiao Y-S, Peterson AW, Deng CX, Stegemann JP, Tissue Eng. Part C Methods 2012, 18, 935. [PubMed: 22624791]

[17]. Shrestha B, Stojkova K, Yi R, Anastasio MA, Ye JY, Brey EM, Acta Biomater. 2020, 117, 374. [PubMed: 33010515]

[18]. Zhang M, Wang Z, Huang P, Jiang G, Xu C, Zhang W, Guo R, Li W, Zhang X, Nanophotonics 2020, 9, 2063.

[19]. Artzi N, Oliva N, Puron C, Shitreet S, Artzi S, bon Ramos A, Groothuis A, Sahagian G, Edelman ER, Nat. Mater 2011, 10, 890. [PubMed: 21892179]

[20]. Wang W, Liu J, Li C, Zhang J, Liu J, Dong A, Kong D, J. Mater. Chem. B 2014, 2, 4185. [PubMed: 32261752]

[21]. Cheng Z, Chai R, Ma P, Dai Y, Kang X, Lian H, Hou Z, Li C, Lin J, Langmuir 2013, 29, 9573. [PubMed: 23829598]

[22]. Jalani G, Naccache R, Rosenzweig DH, Lerouge S, Haglund L, Vetrone F, Cerruti M, Nanoscale 2015, 7, 11255. [PubMed: 26067274]

[23]. Dong Y, Jin G, Ji C, He R, Lin M, Zhao X, Li A, Lu TJ, Xu F, Acta Biomater. 2017, 55, 410. [PubMed: 28428038]

[24]. Zhu W, Chu C, Kuddannaya S, Yuan Y, Walczak P, Singh A, Song X, Bulte JWM, Adv. Funct. Mater 2019, 29, 1903753. [PubMed: 32190034]

[25]. Mertens ME, Hermann A, Bühren A, Olde-Damink L, Möckel D, Gremse F, Ehling J, Kiessling F, Lammers T, Adv. Funct. Mater 2013, 24, 754.

[26]. Chen Z, Yan C, Yan S, Liu Q, Hou M, Xu Y, Guo R, Theranostics 2018, 8, 1146. [PubMed: 29464005]

[27]. Hu S, Zhou Y, Zhao Y, Xu Y, Zhang F, Gu N, Ma J, Reynolds MA, Xia Y, Xu HHK, Tissue Eng J. Regen. Med 2018, 12, e2085.

[28]. Forton SM, Latourette MT, Parys M, Kiupel M, Shahriari D, Sakamoto JS, Shapiro EM, ACS Biomater. Sci. Eng 2016, 2, 508. [PubMed: 30035211]

[29]. Finamore TA, Curtis TE, Tedesco JV, Grandfield K, Roeder RK, Nanoscale 2019, 11, 4345. [PubMed: 30793721]

[30]. Uman S, Wang LL, Thorn SL, Liu Z, Duncan JS, Sinusas AJ, Burdick JA, Adv. Healthc. Mater 2020, 9, 2000294.

[31]. Cole LE, Ross RD, Tilley JM, Vargo-Gogola T, Roeder RK, Nanomedicine 2015, 10, 321. [PubMed: 25600973]

[32]. Hsu JC, Nieves LM, Betzer O, Sadan T, Noel PB, Popovtzer R, Cormode DP, WIREs Nanomed. Nanobiotechnol 2020, 12, e1642.

[33]. Thoniyot P, Tan MJ, Karim AA, Young DJ, Loh XJ, Adv. Sci 2015, 2, 1400010.

[34]. Yadid M, Feiner R, Dvir T, Nano Lett. 2019, 19, 2198. [PubMed: 30884238]

[35]. Clasky AJ, Watchorn JD, Chen PZ, Gu FX, Acta Biomater. 2021, 122, 1. [PubMed: 33352300]

[36]. Heo DN, Ko W-K, Bae MS, Lee JB, Lee D-W, Byun W, Lee CH, Kim E-C, Jung B-Y, Kwon IK, J. Mater. Chem. B 2014, 2, 1584. [PubMed: 32261377]

[37]. Navaei A, Saini H, Christenson W, Sullivan RT, Ros R, Nikkhah M, Acta Biomater. 2016, 41, 133. [PubMed: 27212425]

[38]. Celikkin N, Mastrogiacomo S, Walboomers XF, Swieszkowski W, Polymers 2019, 11, 367.

[39]. Li J, Mooney DJ, Nat. Rev. Mater 2016, 1, 16071. [PubMed: 29657852]

[40]. Castaneda L, Valle J, Yang N, Pluskat S, Slowinska K, Biomacromolecules 2008, 9, 3383. [PubMed: 18959440]

[41]. Schuetz T, Richmond N, Harmon ME, Schuetz J, Castaneda L, Slowinska K, Colloids Surf. B Biointerfaces 2013, 101, 118. [PubMed: 22796781]

[42]. Marcelo G, López-González M, Mendicuti F, Tarazona MP, Valiente M, Macromolecules 2014, 47, 6028.

[43]. Lee D, Heo DN, Nah HR, Lee SJ, Ko W-K, Lee JS, Moon H-J, Bang JB, Hwang Y-S, Reis RL, Kwon IK, Int. J. Nanomed 2018, 13, 7019.

[44]. Ross RD, Cole LE, Tilley JMR, Roeder RK, Chem. Mater 2014, 26, 1187.

[45]. Dong YC, Hajfathalian M, Maidment PSN, Hsu JC, Naha PC, Si-Mohamed S, Breuilly M, Kim J, Chhour P, Douek P, Litt HI, Cormode DP, Sci. Rep 2019, 9, 14912. [PubMed: 31624285]

[46]. Marbella LE, Millstone JE, Chem. Mater 2015, 27, 2721.

[47]. Jain PK, Lee KS, El-Sayed IH, El-Sayed MA, J. Phys. Chem. B 2006, 110, 7238. [PubMed: 16599493]

[48]. Fairbanks BD, Schwartz MP, Bowman CN, Anseth KS, Biomaterials 2009, 30, 6702. [PubMed: 19783300]

[49]. Loessner D, Meinert C, Kaemmerer E, Martine LC, Yue K, Levett PA, Klein TJ, Melchels FPW, Khademhosseini A, Hutmacher DW, Nat. Protoc 2016, 11, 727. [PubMed: 26985572]

[50]. Krause W, Adv. Drug Delivery Rev 1999, 37, 159.

[51]. Ouyang L, Armstrong JP, Lin Y, Wojciechowski JP, Lee-Reeves C, Hachim D, Zhou K, Burdick JA, Stevens MM, Sci. Adv 2020, 6, eabc5529. [PubMed: 32948593]

[52]. Bai X, Gao M, Syed S, Zhuang J, Xu X, Zhang XQ, Bioactive Mater. 2018, 3, 401.

[53]. Piao Y, You H, Xu T, Bei HP, Piwko IZ, Kwan YY, Zhao X, Eng. Regen 2021, 2, 47.

[54]. Zhu K, Shin SR, van Kempen T, Li Y, Ponraj V, Nasajpour A, Mandla S, Hu N, Liu X, Leijten J, Lin Y, Hussain MA, Zhang YS, Tamayol A, Khademhosseini A, Adv. Funct. Mater 2017, 27, 1605352. [PubMed: 30319321]

[55]. Li Q, Zhang B, Xue Q, Zhao C, Luo Y, Zhou H, Ma L, Yang H, Bai D, Int. J. Bioprinting 2021, 7, 394.

[56]. Cetnar AD, Tomov ML, Ning L, Jing B, Theus AS, Kumar A, Wijntjes AN, Bhamidipati SR, Do KP, Mantalaris A, Oshinski JN, Avazmohammadi R, Lindsey BD, Bauser-Heaton HD, Serpooshan V, Adv. Healthc. Mater 2021, 10, e2001169. [PubMed: 33274834]

[57]. Nichol JW, Koshy ST, Bae H, Hwang CM, Yamanlar S, Khademhosseini A, Biomaterials 2010, 31, 5536. [PubMed: 20417964]

[58]. Yin J, Yan M, Wang Y, Fu J, Suo H, ACS Appl. Mater. Interfaces 2018, 10, 6849 [PubMed: 29405059]

[59]. Nguyen AK, Goering PL, Reipa V, Narayan RJ, Biointerphases 2019, 14, 021007. [PubMed: 31053032]

[60]. Ning L, Betancourt N, Schreyer DJ, Chen X, ACS Biomater. Sci. Eng 2018, 12, 3906.

[61]. Ning L, Yang B, Mohabatpour F, Betancourt N, Sarker MD, Papagerakis P, Chen X, Biofabrication 2020, 12, 025011. [PubMed: 31805544]

[62]. Wang X, Ai A, Yu Z, Deng M, Liu W, Zhou G, Li W, Zhang W, Cao Y, Wang X, Mater. Sci. Eng. C 2020, 107, 110307.

[63]. Talacua H, Söntjens SHM, Thakkar SH, Brizard AMA, Herwerden LA, Vink A, Almen GC, Dankers PYW, Bouten CVC, Budde RPJ, Janssen HM, Kluin J, Macromol. Biosci 2020, 20, 2000024.

[64]. Pawelec KM, Chakravarty S, Hix JML, Perry KL, van Holsbeeck L, Fajardo R, Shapiro EM, ACS Biomater. Sci. Eng 2021, 7, 718. [PubMed: 33449622]

[65]. Goth W, Lesicko J, Sacks MS, Tunnell JW, Annu. Rev. Biomed. Eng 2016, 18, 357. [PubMed: 27420574]

[66]. Shirahama H, Lee BH, Tan LP, Cho N-J, Sci. Rep 2016, 6, 31036. [PubMed: 27503340]

[67]. Cui H, Miao S, Esworthy T, Zhou X, Lee S, Liu C, Yu Z, Fisher JP, Mohiuddin M, Zhang LG, Adv. Drug Delivery Rev 2018, 132, 252.

[68]. Rahali K, Messaoud GB, Kahn CJF, Sanchez-Gonzalez L, Kaci M, Cleymand F, Fleutot S, Linder M, Desobry S, Arab-Tehrany E, Int. J. Mol. Sci 2017, 18, 2675.

[69]. Oliver WC, Pharr GM, J. Mater. Res 2004, 19, 3.

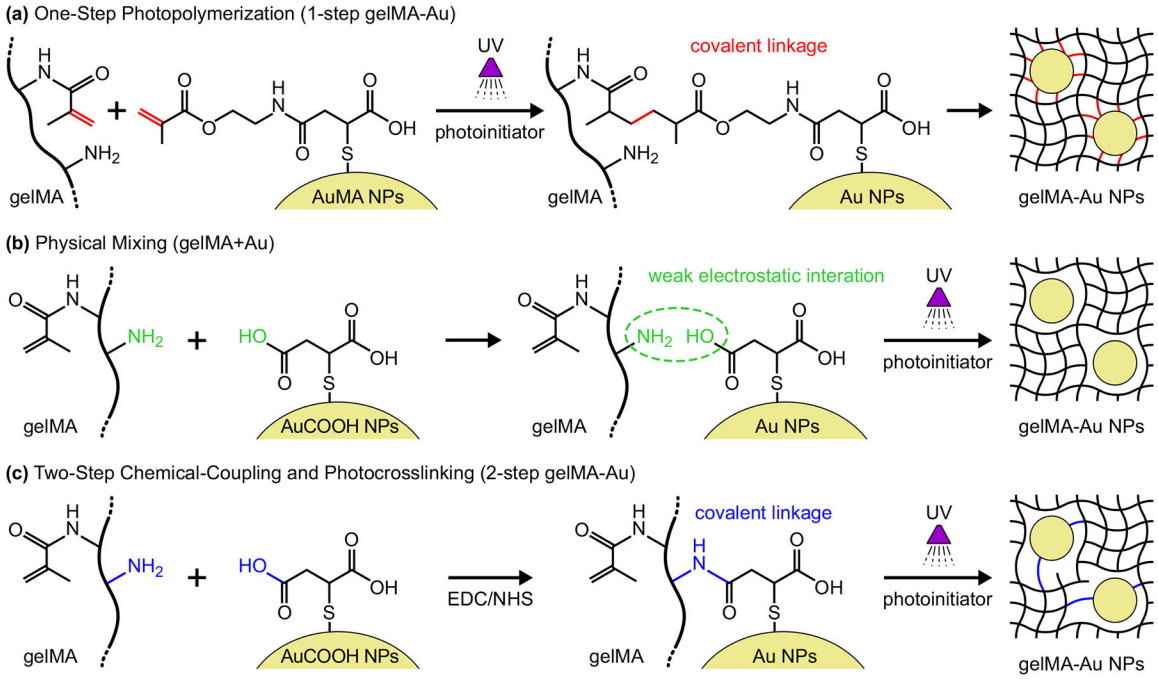

Figure 1. Schemes for the preparation of photopolymerized gelMA-Au NP hydrogels:
(a) one-step photopolymerization of gelMA and AuMA NPs (1-step gelMA-Au) to form covalent linkages, (b) mixing gelMA and AuCOOH NPs (gelMA+Au) with weak electrostatic interactions to physically-entrap Au NPs within the gelMA network, and (c) two-step chemical-coupling and photocrosslinking (2-step gelMA-Au) where covalent linkages between gelMA macromolecules and AuCOOH NPs are formed by EDC/NHS chemistry prior to photocrosslinking gelMA.

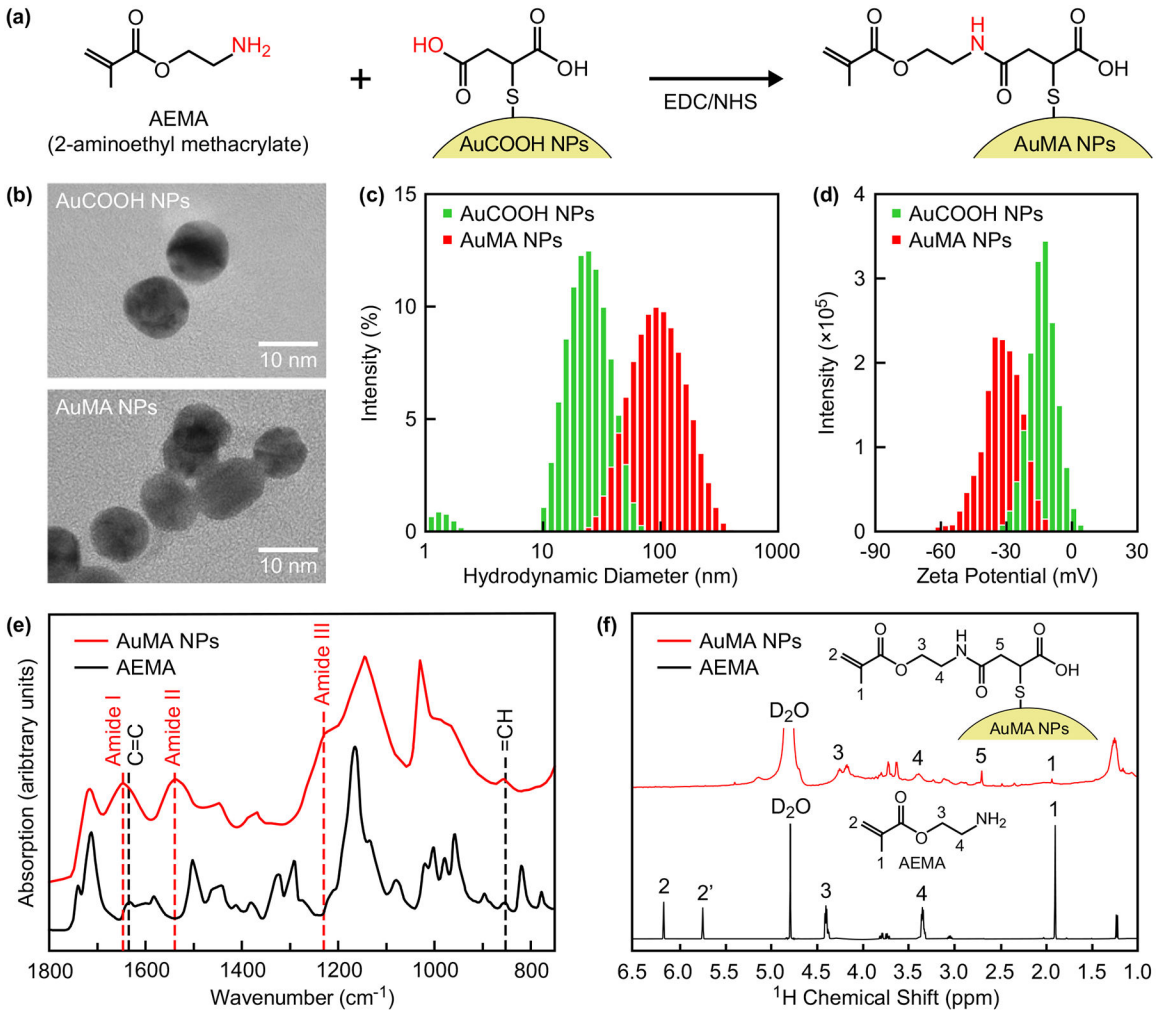

Figure 2. Synthesis and characterization of AuMA NPs.

(a) Scheme for the preparation of AuMA NPs by covalently linking AEMA with AuCOOH NPs using EDC/NHS chemistry. (b) Representative TEM micrographs showing as-prepared AuCOOH and AuMA NPs, which were both spherical and well-dispersed, although AuMA NPs formed dispersible nanoclusters in aqueous solution. The (c) hydrodynamic diameter and (d) zeta potential distributions of as-prepared AuCOOH and AuMA NPs measured by DLS, which confirmed solubility and colloidal stability in aqueous solution. The long-term colloidal stability of AuMA NPs in aqueous solution is shown in Figure S1. (e) FTIR and (f) ^{1}H NMR spectra of as-prepared AuMA NPs compared with AEMA, which verified methacrylate surface modification.

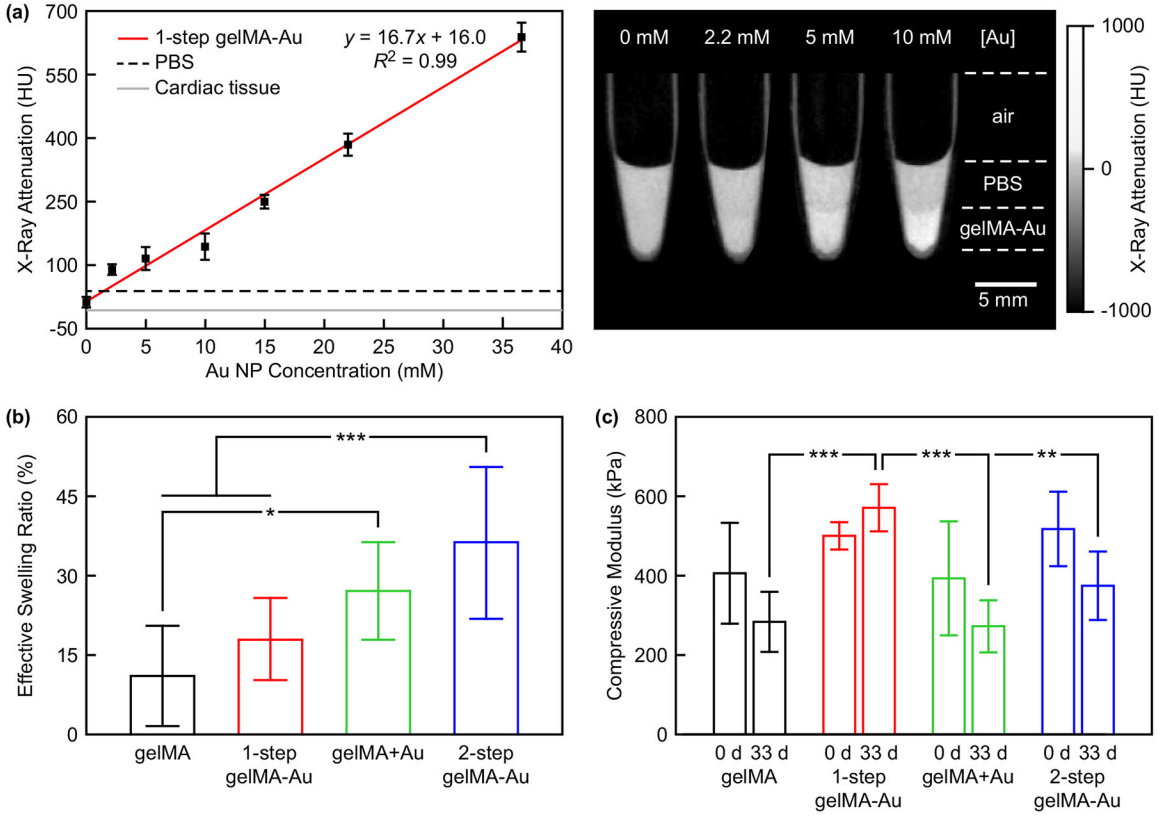

Figure 3. Characterization of gelMA-Au NP hydrogels.

(a) The X-ray attenuation of gelMA-Au NP hydrogels prepared with varying concentration of AuMA NPs by one-step photopolymerization (1-step gelMA-Au) compared with soft tissue, as represented by PBS (38.3 HU) and rat myocardial tissue (−9.3 HU). The measured X-ray attenuation increased linearly with increased Au NP concentration ($p < 0.001$) and was strongly correlated ($R^2 = 0.99$). Error bars show one standard deviation of the mean ($n = 3$/concentration). Grayscale micro-CT images showed that hydrogels containing at least 5 mM Au NPs exhibited visibly greater X-ray attenuation compared with PBS. (b) The effective swelling ratio of gelMA and gelMA-Au NP hydrogels after reaching equilibrium swelling ($n = 10$/group). The effective swelling ratio of 1-step gelMA-Au hydrogels was not statistically different from gelMA alone ($p > 0.48$, Tukey), but was greater for other gelMA-Au hydrogels compared with gelMA. (c) The compressive modulus of gelMA and gelMA-Au NP hydrogels measured before (0 d) and after 33 days hydrolysis ($n =$ 3–5/group/time point). The compressive modulus of as-prepared gelMA and gelMA-Au hydrogels was not different ($p > 0.41$, ANOVA), but was maintained and greater for 1-step gelMA-Au hydrogels, compared to other groups after 33 days hydrolysis. Error bars show one standard deviation of the mean. *$p < 0.05$, **$p < 0.01$, ***$p < 0.005$, Tukey.

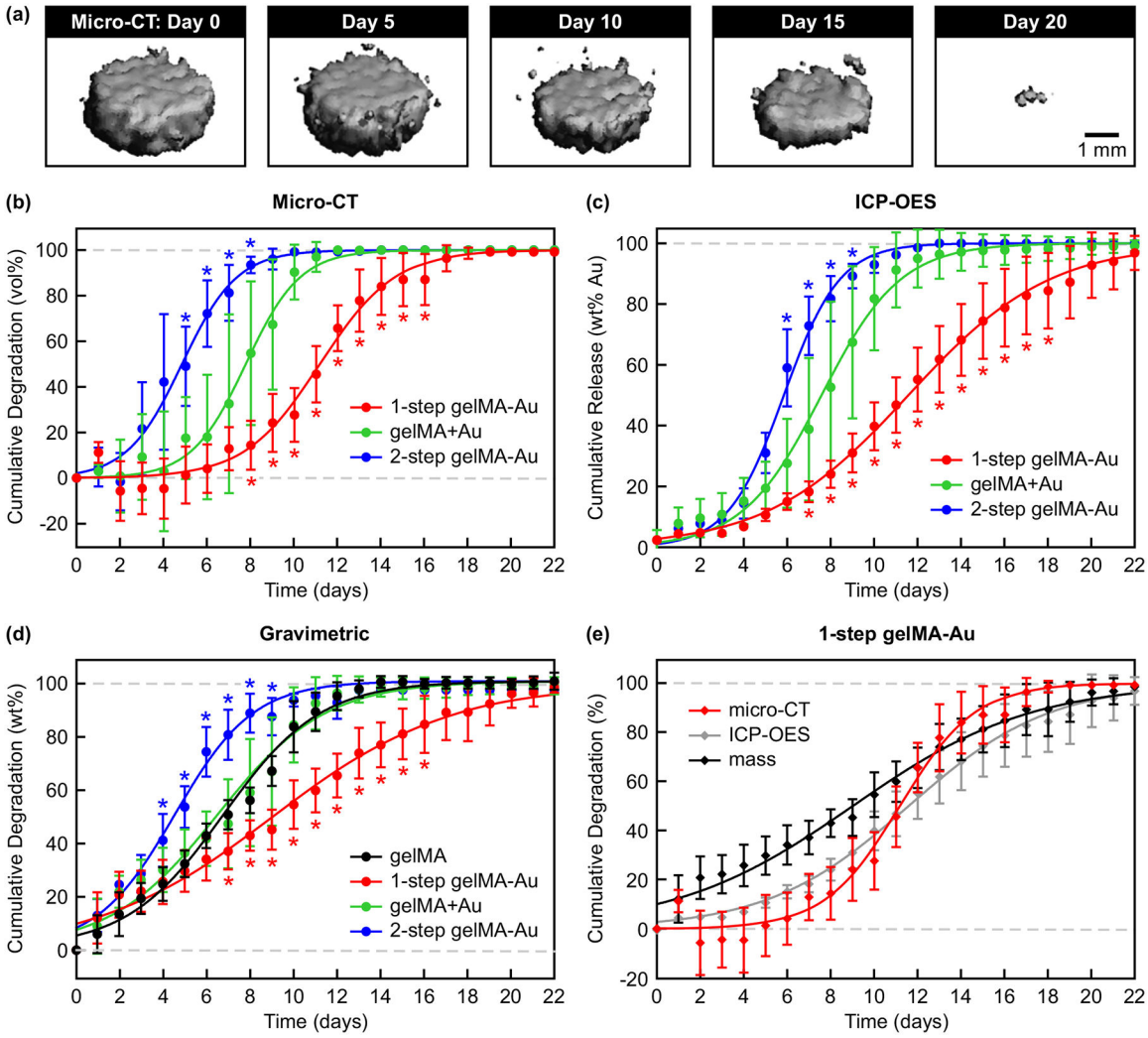

Figure 4. Non-invasive monitoring of gelMA and gelMA-Au NP hydrogels during *in vitro* enzymatic degradation by contrast-enhanced micro-CT.

(a) Representative segmented micro-CT image reconstructions for selected time points showing the volume loss of 1-step gelMA-Au hydrogels during enzymatic degradation. Degradation kinetics were measured longitudinally by (b) the cumulative change in segmented hydrogel volume using contrast-enhanced micro-CT, (c) the cumulative release of Au NPs into the media using ICP-OES, and (d) the cumulative hydrogel mass loss using gravimetric analysis. 1-step gelMA-Au hydrogels exhibited slower degradation kinetics, while 2-step gelMA-Au hydrogels exhibited more rapid degradation kinetics, compared with gelMA and gelMA+Au hydrogels. (e) Comparison of the degradation kinetics for 1-step gelMA-Au hydrogels measured longitudinally by micro-CT, ICP-OES, and gravimetric analysis. The degradation kinetics measured by micro-CT were strongly correlated ($r > 0.96$, Pearson) with that measured by ICP-OES and gravimetric analysis, demonstrating the feasibility of contrast-enhanced micro-CT for non-invasive monitoring of gelMA-Au NP hydrogel degradation. Degradation kinetics were modeled by non-linear least squares regression using a four-parameter logistic model (Equation 1) with fitting parameters reported in Table 1. Error bars show one standard deviation of the mean ($n = 5$/group).

Error bars not shown lie within the data point. *$p < 0.05$ vs. gelMA+Au in (b,c), vs. gelMA in (d), vs. micro-CT and ICP-OES in (e) Tukey.

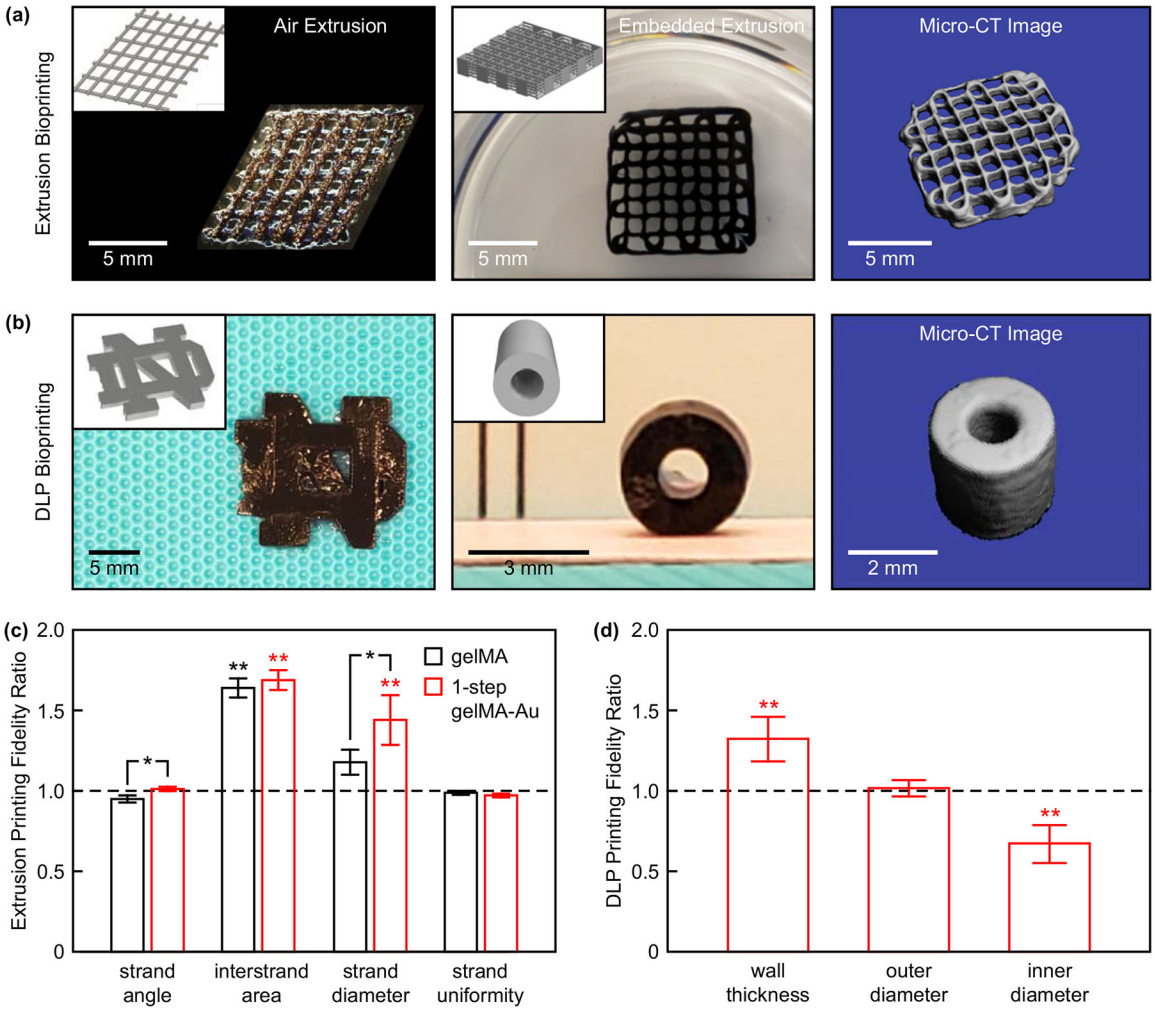

Figure 5. 3D bioprinting of 1-step gelMA-Au NP hydrogel constructs.

(a) A two-layer lattice scaffold printed by air extrusion and 10-layer lattice scaffold printed by embedded extrusion. (b) The University of Notre Dame logo (left) and a cylindrical tube mimicking a blood vessel printed by DLP bioprinting. Insets show corresponding CAD models. Segmented micro-CT image reconstructions of the 10-layer lattice scaffold and cylindrical tube show feasibility of non-invasive radiograph imaging. (c) Microscale printing fidelity measured for two-layer lattice scaffolds printed by air extrusion with gelMA and 1-step gelMA-Au hydrogels. The printing fidelity of 1-step gelMA-Au hydrogels was comparable to that of gelMA alone. Error bars show one standard deviation of the mean (n = 5/group). (d) Macroscale printing fidelity measured for cylindrical tubes printed by DLP bioprinting with 1-step gelMA-Au hydrogels. Error bars show one standard deviation of the mean (n = 9/group). In (c) and (d), a ratio of one (dashed line) indicates no deviation from the CAD models. *$p < 0.05$, Tukey. **$p < 0.005$ vs. 1, exact t-test.

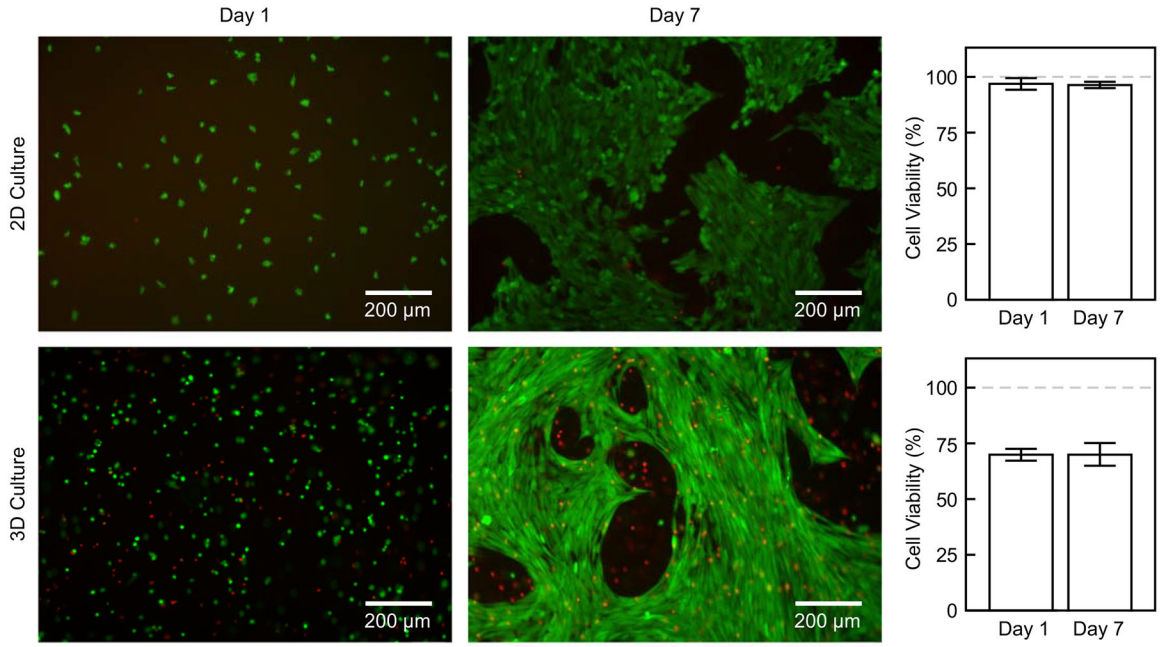

Figure 6. Cell viability in 3D bioprinted 1-step gelMA-Au NP hydrogel constructs.

Representative epifluorescence micrographs showing live(green)/dead(red) staining of HUVECs after 1 and 7 days of 2D and 3D culture with 1-step gelMA-Au hydrogels. Quantitative measurements showed more than 95% viable cells in 2D culture and more than 70% viable cells in 3D culture. There was no loss of viability over 7 days culture ($p > 0.71$, ANOVA).

Table 1.

Non-linear least squares regression of gelMA and gelMA-Au NP hydrogel enzymatic degradation kinetics using a four-parameter logistic model (Equation 1), where t_{50} is the degradation half-life, including the 95% confidence interval (CI), H is the Hill slope or steepness of the kinetic curves which reflects the hydrogel degradation rate, and R^2 is the model correlation coefficient.

Group	Test Method	t_{50} (days)	t_{50}, 95% Cl	H	R^2
gelMA	gravimetric	6.8	6.6 – 7.0	0.19	0.98
	micro-CT	11.2	10.9 – 11.5	0.25	0.95
1-step gelMA-Au	ICP-OES	11.6	11.3 – 11.9	0.13	0.95
	gravimetric	9.0	8.7 – 9.4	0.11	0.94
	micro-CT	7.8	7.4 – 8.1	0.35	0.89
gelMA+Au	ICP-OES	7.6	7.3 – 7.9	0.24	0.92
	gravimetric	6.5	6.2 – 6.8	0.18	0.93
	micro-CT	4.8	4.6 – 5.1	0.34	0.94
2-step gelMA-Au	ICP-OES	5.9	5.8 – 6.0	0.34	0.99
	gravimetric	4.5	4.4 – 4.7	0.24	0.97